sustainability

IMPACT FACTOR 4.1

CITESCORE 8.9

Article

Digital Twin Based Optimal Design of a Grid-Connected Hybrid Renewable Energy Microgrid Using Improved Multi-Objective Optimization: A Case Study

Shasha Li, Chee Wei Tan and Nedim Tutkun

Special Issue

Advances in Renewable Energy and Power Generation Technology

Edited by

Dr. Zsolt Čonka

MDPI

https://doi.org/10.3390/su18136532

sustainability

MDPI

Article

Digital Twin Based Optimal Design of a Grid-Connected Hybrid Renewable Energy Microgrid Using Improved Multi-Objective Optimization: A Case Study

Shasha Li [1], Chee Wei Tan [1,*] and Nedim Tutkun [2]

[1] Department of Electrical Power Engineering, Faculty of Electrical Engineering, Universiti Teknologi Malaysia, UTM Skudai, Johor Bahru 81310, Johor Darul Takzim, Malaysia; lishasha@graduate.utm.my
[2] Department of Electrical and Electronics Engineering, Faculty of Engineering, Istanbul Ticaret University, Maltepe, İstanbul 34840, Türkiye; ntutkun@ticaret.edu.tr
* Correspondence: cheewei@utm.my

Abstract

This study investigates the optimal sizing of a grid-connected hybrid renewable energy microgrid. The optimization, employing a multi-objective artificial hummingbird algorithm (MOAHA) combined with fuzzy decision-making (FDM), aims to minimize the cost of energy while maximizing renewable energy utilization. MOAHA is used to generate a well-distributed Pareto front, while FDM identifies the preferred configuration under the specified decision preference. However, the preferred solution obtained is a static configuration. Most existing studies focus on such static planning, with limited attention to dynamic mapping and validation of the optimized configuration. To bridge this gap, a digital twin architecture is further proposed for hybrid renewable energy microgrids, and a corresponding digital twin system is also developed to achieve virtual representation, dynamic state mapping, operational visualization, and configuration validation. An industrial park microgrid in Urumqi is selected as the case study. The results indicate that the preferred configuration achieves a cost of energy of 0.065 $/kWh and a renewable energy utilization of 0.675. Comparative results demonstrate that the proposed framework outperforms benchmark methods in terms of convergence, solution diversity, and computational efficiency. Meanwhile, the developed digital twin system effectively supports time-series state visualization and feasibility checking of the optimized configuration.

Keywords: hybrid renewable microgrid; sizing optimization; multi-objective artificial hummingbird algorithm; fuzzy decision; digital twin

Check for updates

Academic Editor: Zsolt Čonka

Received: 20 May 2026
Revised: 15 June 2026
Accepted: 22 June 2026
Published: 26 June 2026

Copyright: © 2026 by the authors. Licensee MDPI, Basel, Switzerland. This article is an open access article distributed under the terms and conditions of the Creative Commons Attribution (CC BY) license.

1. Introduction

Energy systems are consuming increasing amounts of electricity and require a stable and reliable power supply. The transformation of energy systems is becoming increasingly important because modern power systems must simultaneously satisfy growing electricity demand, reduce carbon emissions, and maintain secure energy supply. Renewable energy resources play a key role in this transition because they can reduce dependence on traditional fossil fuels. However, a power system cannot only rely on intermittent renewable resources. Therefore, the integration of traditional energy sources or the utility grid with renewable energy is necessary. Such integration can provide dispatchable power support when renewable generation is insufficient, improve system reliability, and reduce the operational risks. However, renewable sources are variable and uncertain due to their

dependence on solar irradiation, wind speed, and weather conditions [1]. The intermittency of renewable energy also introduces several technical and operational challenges. Solar and wind power outputs change with weather conditions and may not match the temporal variation in load demand. This mismatch can lead to power imbalance, frequent battery charging and discharging, increased grid power exchange, renewable energy curtailment, and higher operating costs. From the perspective of system operation, large fluctuations in renewable generation may also affect voltage stability, frequency regulation, and the reliability of power supply, particularly when the storage system reaches its limits or when load demand increases rapidly [2]. Therefore, renewable energy microgrid planning should not only determine the optimal capacities of key components, but evaluate whether the selected configuration can maintain stable operation [3].

Hybrid renewable energy microgrids (HREMs) are a promising solution for energy systems. An HREM usually integrates photovoltaic (PV), wind turbines (WT), battery energy storage systems (BESS), and the utility grid, and can operate in grid-connected or islanded mode. Compared with single-source renewable energy systems, HREMs can make better use of the characteristics of different renewable resources. For example, a PV/WT/BESS-based hybrid microgrid optimization framework was proposed by [4] to coordinate renewable generation and energy storage, with the objective of reducing energy losses, voltage fluctuations, and power purchased from the main grid. An optimal dimensioning model for a grid-connected PV/wind hybrid renewable energy system with battery and supercapacitor storage was developed by [5], aiming to reduce annual system cost while maintaining renewable energy utilization. A grid-connected PV/wind/battery microgrid optimization model was investigated by [6] to determine cost-effective hybrid configurations. However, the planning of an HREM is not straightforward. The system involves multiple components and operating constraints. Moreover, different planning objectives often conflict with each other. For example, increasing the capacities of PV, WT, and BESS can improve renewable energy utilization, but it may also increase the system cost. Therefore, HREM sizing is a typical multi-objective decision problem that requires an effective optimization method.

Existing studies have employed various optimization algorithms for the sizing of renewable energy systems. These methods can provide a set of Pareto-optimal solutions for engineers. For instance, a hybrid NSGA-II and grey wolf optimizer was proposed by [7] to determine the optimal combination of wind, PV, and battery capacities for a hybrid microgrid. A multi-objective optimization framework was developed by [8] for an off-grid hybrid renewable energy system, considering economic, reliability, environmental, and social objectives. An improved NSGA-II method was proposed by [9] for a hydrogen-integrated hybrid renewable energy system, with the objective of optimizing system cost, efficiency, and reliability. However, after obtaining the Pareto front, multiple mutually non-dominated solutions still remain, making it difficult to select a personalized final configuration according to engineer preferences.

As mentioned before, existing HREM planning studies mainly focus on obtaining an optimized sizing scheme, while the selected configuration is usually treated as a static result. Such a static scheme cannot directly reflect the dynamic operational behavior of the planned microgrid. As a result, there remains a gap between the planning result and its dynamic operational performance.

To solve these problems, this study proposed an integrated framework for the optimal planning and dynamic validation of an HREM, which combines a multi-objective artificial hummingbird algorithm (MOAHA) and fuzzy decision-making (FDM) optimization framework with a digital twin system. In the optimization stage, MOAHA is employed to conduct global search and generate a Pareto solution set with good convergence and diver-

sity. FDM is then used to evaluate and rank the candidate solutions based on membership functions and preference weights, enabling engineer to identify a practical sizing scheme from the Pareto set according to their specific requirements. In the validation stage, this paper further proposed a digital twin architecture and developed a corresponding digital twin system for the optimized HREM configuration. The digital twin provides a virtual representation of the physical microgrid and enables dynamic state mapping, operational visualization, and performance validation.

From the planning perspective, the proposed framework can help engineers compare the trade-off between economic cost and renewable energy utilization, and allocate investment among PV, WT, and BESS in a more systematic way. Additionally, from the operational perspective, the optimized configuration is not only presented as a static sizing result but is further mapped into a digital twin environment to examine its dynamic behavior under hourly variations in renewable generation, load demand, battery SOC, and grid interaction. Therefore, the proposed framework can support practical decision-making, reduce the risk of directly implementing an unverified configuration, and provide useful operational insights for industrial park microgrid planning, energy management, and low-carbon energy transition. As a result, the main contributions of this study are as follows:

- A MOAHA-FDM optimization framework is proposed for the sizing of hybrid renewable microgrids. Different from optimization only frameworks that mainly generate Pareto fronts, the proposed framework combines MOAHA Pareto front generation with FDM preference ranking. MOAHA is adopted because its external archive and dynamic elimination-based crowding distance mechanism help improve convergence and solution diversity, while FDM further transforms multiple non-dominated solutions into a final preferred configuration according to engineering preferences;
- A digital twin architecture for hybrid renewable energy microgrids is proposed, and a corresponding digital twin system is developed to map the optimized configuration into a dynamic virtual environment, enabling time-series state visualization, operational feasibility checking, and validation of the planning result before practical implementation;
- The proposed optimization framework and digital twin architecture are applied to a grid-connected industrial park microgrid in Urumqi. The preferred configuration achieves a COE of 0.065 $/kWh and an REF of 0.675, and the digital twin system further verifies the operational feasibility of the optimized configuration through dynamic visualization of PV output, WT output, load demand, battery state of charge (SOC), and grid interaction.

The rest of this paper is organized as follows. Section 2 models the microgrid components. Section 3 formulates the optimization problem. The proposed joint optimization framework is presented in Section 4. Section 5 describes the operating modes of the rule-based energy management strategy. The proposed digital twin architecture for the microgrid is introduced in Section 6. Section 7 provides the case study location and input parameters. The optimization results and digital twin system analysis are given in Section 8. Finally, Section 9 concludes the paper.

2. Modeling of the Microgrid Components

As illustrated in Figure 1, this study considers a grid-connected hybrid renewable energy microgrid, which consists of PV, WT, a BESS, an inverter, and the utility grid.

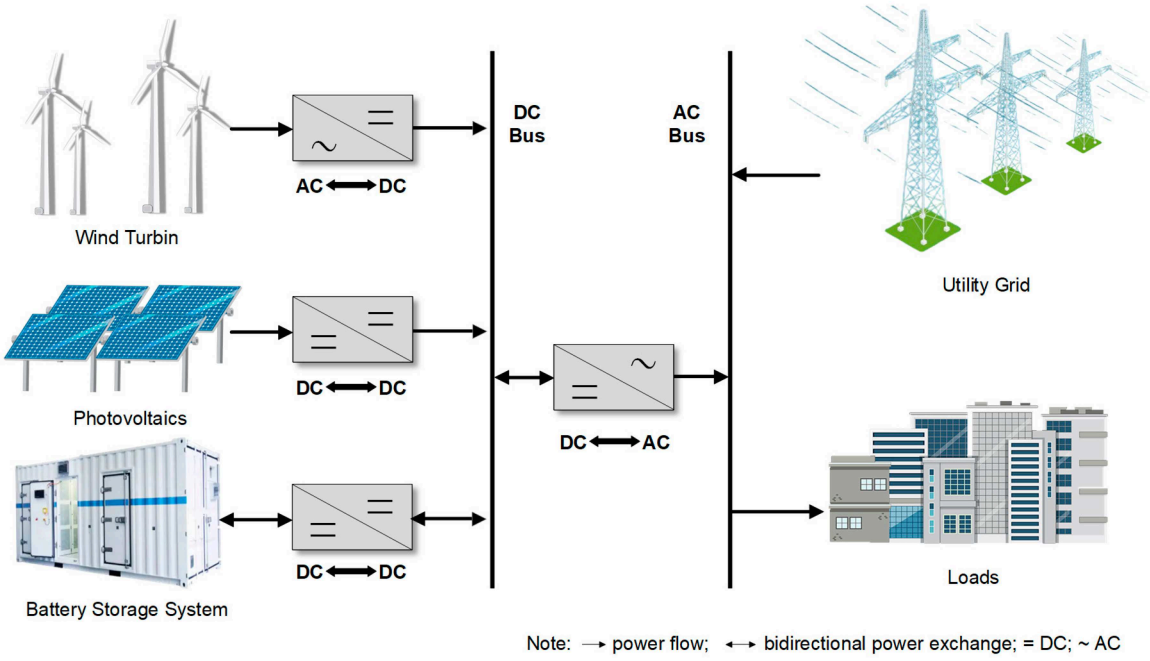


Figure 1. The hybrid renewable energy microgrid considered in this paper.

2.1. Photovoltaic System

The PV system can transform solar energy into electricity. The PV output electricity can be calculated as follows [10]:

$$P_{PV-out}(t) = P_{N-PV} \times \frac{G}{G_{ref}} \times \left[1 + K_t \times \left((T_{amb} + (0.025 \times G)) - T_{ref}\right)\right] \quad (1)$$

where $P_{PV-out}(t)$ represents the PV output at time t. P_{N-PV} indicates the nominal power of the PV under standard test conditions. G is the solar irradiance. G_{ref} is 1 kW/m^2; K_t represents a constant with a value of -3.7×10^{-3} (1/°C). T_{amb} indicates the ambient temperature, and T_{ref} denotes the reference temperature (25 °C).

2.2. Wind Turbine

The wind speed mainly depends on height. The wind speed in hub height can be expressed as follows [11]:

$$\frac{v_{WT}}{v_1} = \left(\frac{h_{WT}}{h_1}\right)^{\alpha} \quad (2)$$

where v_1 and v_{WT} represents the wind speed at the reference height h_1 and the wind turbine hub height h_2, and α indicates the friction coefficient, which depends on terrain, surface roughness, and other environmental factors. The output of WT can be determined as follows:

$$P_{WT-out}(v_{WT}) = \begin{cases} 0, & v_{WT} < v_{cut-in} \text{ or } v_{WT} > v_{cut-out} \\ P_{rated} \times \frac{v_{WT}^3 - v_{cut-in}^3}{v_{rated}^3 - v_{cut-in}^3}, & v_{cut-in} \le v_{WT} < v_{ratet} \\ P_{rated}, & v_{ratet} \le v_{WT} < v_{cut-out} \end{cases} \quad (3)$$

where P_{rated}. is the rated power of the wind turbine, v_{WT} denotes the wind turbine hub-height wind speed at the current time, v_{cut-in} and $v_{cut-out}$ are the cut-in and cut-out wind speeds of the turbine, and v_{ratet} represents the rated wind speed of the turbine.

2.3. Battery Energy Storage System

The BESS can be used to store the surplus energy generated by renewable sources and discharge it when renewable generation cannot meet the load demand. The factor that indicates the battery's charging or discharging states is the SOC. It is formulated as follows:

$$SOC(t) = SOC(t-1) + \frac{\eta_{ch} \times P_{BESS}^{ch}(t) - \frac{P_{BESS}^{dis}(t)}{\eta_{dis}}}{C_B} \times \Delta t \quad (4)$$

$$SOC_{\min} \leq SOC(t) \leq SOC_{\max} \quad (5)$$

where $P_{BESS}^{ch}(t)$ and $P_{BESS}^{dis}(t)$ is the charging and discharging power of the BESS at time t, η_{ch} and η_{dis} is the charging and discharging efficiencies, which typically range from 0.85 to 0.95, and Δt represents the time step duration.

2.4. Inverter

The inverter is responsible for transforming the direct current (DC) generated from PV and BESS into alternating current (AC) to meet the requirement of AC load or grid connection. The efficiency of inverter can be measured as follows [12]:

$$\eta_{inv} = \frac{P}{P + P_0 + kP^2} \quad (6)$$

$$P = \frac{P_{out}}{P_n} \quad (7)$$

$$P_0 = 1 - 99 \times \left(\frac{10}{\eta_{10}} \times \frac{1}{\eta_{100}} - 9\right)^2 \quad (8)$$

$$k = \frac{1}{\eta_{100}} - P_0 - 1 \quad (9)$$

where P_{out} and P_n represent the actual output and the rated power of the inverter, η_{10} and η_{100} denote the inverter efficiency at 10% and 100% of the nominal power, respectively (provided by the manufacturer).

2.5. Utility Grid

When renewable generation and the battery cannot meet the load demand, electricity is imported from the utility grid to meet the load demand and charge the battery. The imported electricity is modeled based on Equation (10). On the other hand, when surplus energy is generated by renewable sources and the battery is fully charged, the excess energy is exported to the utility grid. The exported electricity is evaluated using Equation (13).

$$P_{Grid_imp}(t) = P_{load}(t) - [P_{PV-out}(t) + P_{WT_out}(t) + [(SoC(t) - SoC_{\min}(t)) \times \eta_{inv}]] \quad (10)$$

$$E_{Grid_imp} = \sum_{t=1}^{8760} P_{Grid_imp}(t) \quad (11)$$

$$C_{Grid_imp} = C_b \times E_{Grid_imp} \quad (12)$$

where $P_{Grid\text{-}imp}$ represents the hourly electricity imported from utility grid, $E_{Grid\text{-}imp}$ is the total imported electricity for one year, C_b indicates the price of importing 1 kWh electricity from utility grid, and $C_{Grid\text{-}imp}$ denotes the total cost of purchasing electricity from utility grid in one year.

$$P_{Grid_exp}(t) = P_{PV-out}(t) + P_{WT_out}(t) + [(SoC(t) - SoC_{\max}(t)) \times \eta_{inv}] - P_{load}(t) \quad (13)$$

$$E_{Grid_\exp} = \sum_{t=1}^{8760} P_{Grid_\exp}(t) \tag{14}$$

$$I_{Grid_\exp} = R_{feed\text{–}in\ tariff} \times E_{Grid_\exp} \tag{15}$$

where $P_{Grid\text{-}exp}$ represents the hourly electricity exported to the utility grid, $E_{Grid\text{-}exp}$ is the total exported electricity for one year, $R_{feed\text{-}in\text{-}tariff}$ indicates the price of exporting 1 kWh electricity to utility grid, and $I_{Grid\text{-}exp}$ refers to the total income of selling electricity to utility grid in one year.

3. Formulation of the Optimization Problem

3.1. Objective Functions

This study formulates a two-objective optimization model to balance energy cost and renewable energy utilization in proposed hybrid renewable energy microgrid.

3.1.1. Cost of Energy

Cost of energy (COE) reflects the ratio of the total lifecycle cost of the system to the total load demand. It relates the total net present cost of the microgrid to the annual energy demand through the capital recovery factor (CRF), thereby accounting for the time value of money [13]. It is formulated as follows:

$$\mathrm{COE}\left(\frac{\$}{\mathrm{kWh}}\right) = \frac{\text{Total Net Present Cost}(\$)}{\sum_{h=1}^{8760} P_{\mathrm{load}}(\mathrm{h})(\mathrm{kWh})} \times \mathrm{CRF} \tag{16}$$

$$\text{Total Net Present cost}(\$) = C_{inv} + C_{OM} + C_{Bess_rep} + C_{Grid_pur} \tag{17}$$

where total net present cost ($) is the total net present cost of the microgrid system during its entire lifecycle. This typically includes the equipment investment cost C_{inv}, operation and maintenance cost C_{OM}, battery replacement cost C_{Bess_rep}, and the cost of purchasing electricity from the utility grid C_{Grid_pur} . The system's revenue obtained from selling electricity to the grid, which is treated as a cash inflow and deducted from the total cost. $\sum_{h\,=\,1}^{h\,=\,8760} P_{\mathrm{load}}(\mathrm{h})$ represents the total electrical load demand of the system over the course of 8760 h in one year, where $P_{\mathrm{load}}(\mathrm{h})$ is the power consumption per hour. The denominator reflects the overall energy supply scale of the system, facilitating the allocation of total cost to each unit of electricity to compute the cost per kWh. The CRF is used to annualize the total investment or net present cost of the microgrid system, accounting for the time value of money. The formula is modeled as follows:

$$\mathrm{CRF} = \frac{r(1+r)^n}{(1+r)^n - 1} \tag{18}$$

where r represents the actual interest rate, and n is the system life period. The primary function of the CRF is to convert future investment or operational expenditure into their present value and transform them into equivalent fixed annual payments.

In practical engineering applications, the actual interest rate r is typically determined based on the national or regional benchmark interest rate, cost of capital, or industry norms, commonly falling within the range of 5% to 10%. The system life period n is usually set according to the design life, maintenance cycle, or contractual duration of key microgrid components. Typical values from 15 to 25 years.

3.1.2. Renewable Energy Factor

Renewable energy factor (REF) represents the proportion of renewable energy generation relative to the total energy supply, including electricity imported from the utility grid. The second objective is to maximize REF, which is calculated as follows [14]:

$$\mathrm{REF} = \left(\frac{\sum P_{WT} + \sum P_{PV}}{\sum P_{WT} + \sum P_{PV} + \sum P_{Grid_pur}} \right) \times 100\% \tag{19}$$

A higher REF value indicates greater renewable energy penetration and a more sustainable microgrid configuration. To facilitate the multi-objective optimization process, all objectives are expressed in a minimization form. Therefore, in the actual algorithm implementation, the second objective is defined as minimizing the negative value of REF, which is equivalent to maximizing the renewable energy factor.

3.2. Problem Constraints

The constraints for the proposed combined multi-objective optimization approach are as follows:

$$P_{PV}(t) + P_{WT}(t) + P_{BESS}^{dis}(t) + P_{Grid_pur}(t) \geq P_{Load}(t) \tag{20}$$

$$SOC_{\min}(t) \leq SOC(t) \leq SOC_{\max}(t) \tag{21}$$

$$PV_{\min} \leq PV \leq PV_{\max} \tag{22}$$

$$WT_{\min} \leq WT \leq WT_{\max} \tag{23}$$

where Equation (20) ensures that the total power supplied by renewable energy sources, battery discharge, and electricity imported from the utility grid is sufficient to meet the load demand at all times. Equation (21) guarantees that the battery operates within its allowable SoC range, thereby ensuring safety and prolonging battery life. A constraint is introduced that the $\mathrm{SoC}_{\min}$ is sufficient to supply the load demand for at least one hour, thereby ensuring system operation during utility grid power outages. Equations (22) and (23) impose capacity constraints on PV and WT systems, respectively, requiring their installed capacities to remain within predefined lower and upper bounds.

3.3. Decision Variables

In this study, the decision variables for multi-objective optimization consist of the nominal power of PV (kW), the capacity of the BESS (kWh), and the number of WTs. The nominal power of PV represents the total rated capacity of the installed PV system. And battery capacity is an indirect indicator for measuring the scale of BESS. By optimizing decision variables, the proposed improved multi-objective optimization algorithm aims to enhance the performance of hybrid renewable energy microgrids in terms of renewable energy factor and economic efficiency.

3.4. Assessment Metrics

3.4.1. Mean Ideal Distance

The mean ideal distance (MID) is used to assess the convergence of solutions towards the ideal point in multi-objective optimization problems. In two-objective optimization, MID measures the average normalized Euclidean distance from each solution to the ideal point across all objectives. The ideal point is composed of the best values achieved for each objective function. A smaller MID value reflects a closer proximity of the Pareto front to

the ideal point, thereby indicating better convergence performance. It is formulated as follows [15]:

$$\mathrm{MID} = \frac{\sum_{i=1}^{n'} \sqrt{\left(\frac{F1_i - F1_{Best}}{F1_{Total}^{Max} - F1_{Total}^{Min}}\right)^2 + \left(\frac{F2_i - F2_{Best}}{F2_{Total}^{Max} - F2_{Total}^{Min}}\right)^2}}{n} \quad (24)$$

where n represents the solution numbers in the Pareto front, $F1_i$ and $F2_i$ are the objective functions' values for the ith solution, $F1_{Best}$ and $F2_{Best}$ represent the ideal values of the respective objectives, and $F1_{Total}^{Max}$, $F1_{Total}^{Min}$, $F2_{Total}^{Max}$ and $F2_{Total}^{Min}$ indicate the maximum and minimum values of each objective function among all obtained solutions.

3.4.2. Diversity Metric

Diversity metric (DM) is utilized to measure the diversity of solutions along the Pareto front. A larger DM value reveals better solution diversity. It is calculated as follows [15]:

$$\mathrm{DM} = \sqrt{\sum_{i=1}^{n} (Min\ F_i - Max\ F_i)^2} \quad (25)$$

where $Min\ F_i$ and $Max\ F_i$ is the minimum and maximum value of each objective function, respectively.

4. Proposed Joint Optimization Framework

As shown in Figure 2, this study proposed a joint framework that combines MOAHA and FDM. MOAHA is used to generate a Pareto-optimal solution set. It improves convergence and solution diversity. Since the Pareto set contains multiple non-dominated solutions, it is difficult to choose one configuration directly. FDM is applied to score and rank the candidate solutions using membership functions. Engineers can assign weights according to their preferences, and the solution with the highest total membership value is selected as the preferred configuration under the specified decision preference.

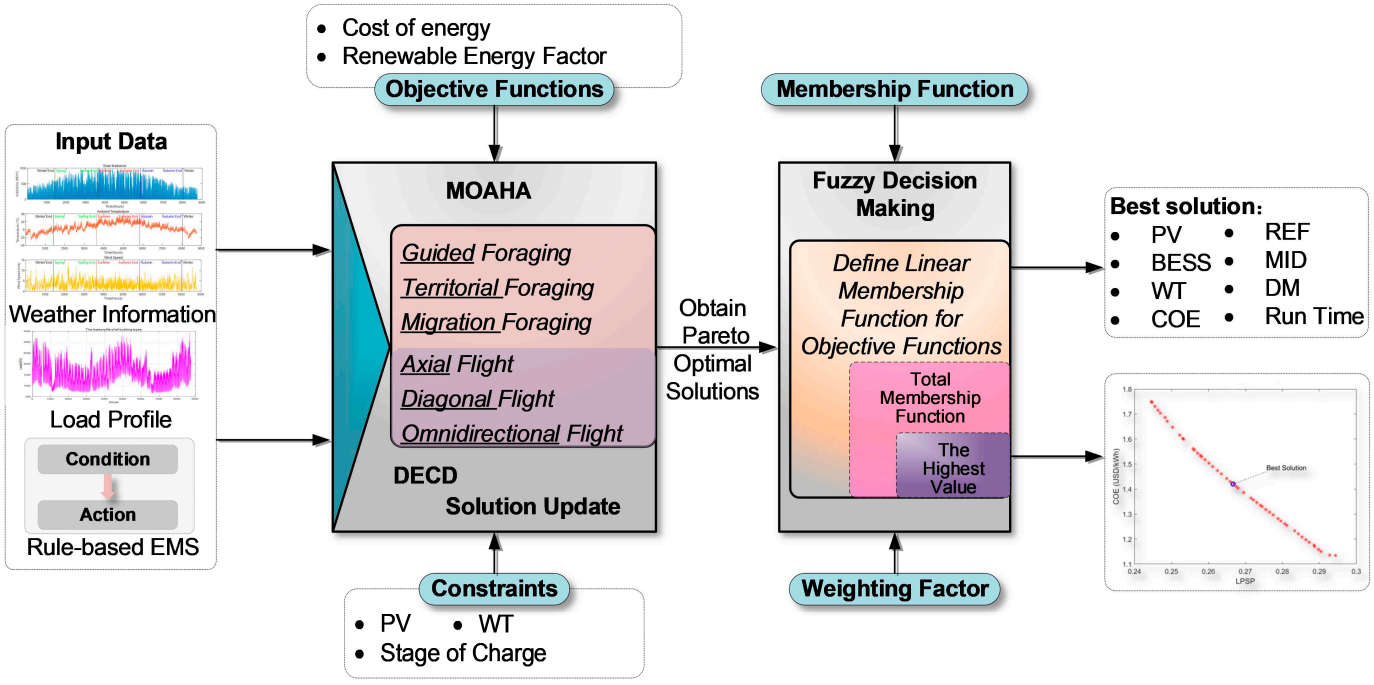


Figure 2. Framework of the proposed improved multi-objective optimization algorithm, red asterisks represent non-dominated candidate solutions on the Pareto front.

From a methodological perspective, MOAHA is suitable for the HREM sizing problem because it provides a good balance between global exploration and local exploitation through its guided, territorial, and migration foraging behaviors, as well as different flight patterns. This is important because the sizing problem involves nonlinear component models, capacity constraints, SOC limits, and conflicting objectives between COE and REF. In addition, the external archive and dynamic elimination-based crowding distance mechanism of MOAHA help maintain the convergence and diversity of Pareto solutions. Furthermore, FDM is introduced to overcome the limitation of optimization only frameworks. Conventional multi-objective algorithms usually stop after generating a set of non-dominated solutions, leaving the final configuration selection to subjective judgment. In contrast, FDM converts the objective values of Pareto solutions into membership values and ranks them according to predefined preference weights. Therefore, the proposed framework provides a complete optimization to decision process, in which MOAHA generates high quality trade-off solutions and FDM selects the final configuration according to engineer preferences.

4.1. Multi-Objective Artificial Hummingbird Algorithm

The multi-objective artificial hummingbird algorithm is proposed to address the multi-objective optimization issues through three key components. An external archive, the first component, is utilized to store a fixed number of non-dominated solutions during the iterative optimization process. The second component is a solution update mechanism. This mechanism first adopts the traditional non-dominated sorting (NDS), in which a solution dominates another solution if it is no worse in all objectives and strictly superior in at least one objective. Based on this principle, the first Pareto front is not dominated by any others solution. After removing the first front, the second Pareto front is determined by the rest of solutions using NDS, and so on. The candidate solution generated by different foraging is compared to current solution based on their corresponding front level. If the candidate solution has better front level, it can replace the current solution. However, when the candidate solution and the current solution have the same Pareto front, MOAHA employs a special update strategy in which the update is determined randomly with 50% to balance the convergency and diversity in optimization process. Also, a dynamic elimination-based crowding distance (DECD) mechanism is adopted to maintain archive diversity and improve computational efficiency during optimization. The crowding distance for all solutions is computed just one time in conventional archiving process. The solutions are sorted based on the aforementioned crowding distance and the solution with smallest crowding distance is removed first.

However, after removing the solution with the smallest crowding distance, the rest of the solutions crowding distances will be changed. If the archive continues to delete solutions based on the original crowding distance without update, it may mistakenly elimination boundary solutions, which will degrade convergence and diversity of the Pareto front. To address the above issue, MOAHA introduces a dynamic elimination-based crowding distance. DECD only removes the current solution with the smallest crowding distance and updates the crowding distance of its neighboring solution, while keeping the crowding distance of the other solutions unchanged. This dynamic update strategy avoids the computational overhead of global computational and enhances the diversity of archives.

4.2. Comparison of MOAHA with Benchmark Algorithms

By evaluating the performance of three representative algorithms with MOAHA under a unified environment across several performance metrics, this comparison highlights

the superior performance of the MOAHA algorithm in terms of solution diversity and convergence performance, thereby laying a solid foundation for the integration of the fuzzy decision-making strategy.

The case study data from Urumqi (in Section 7) are used as input for all four algorithms. To ensure a fair comparison across algorithms and avoid bias from different search spaces, the population size is set to 50, and the number of iterations is fixed at 100. Each algorithm is executed on the same platform (Windows 11, AMD Ryzen 7 8845H, MATLAB R2023b). As the optimization of HRMS is a multi-objective problem, the optimal solutions are presented in the form of a Pareto front, meaning multiple non-dominated solutions exist with varying COE and REF values. In this sector, the solution with the highest crowding distance is selected as the best solution. The details of the obtained results are presented in Table 1.

Table 1. Optimization results of MOAHA and benchmark algorithms.

Optimization Algorithm	PV (kW)	BESS (kWh)	WT (Number)	COE ($)	REF	MID *	DM **	Run Time (s)
NSGA-II	5009.982	6991.641	11	0.066	0.683	1	0.079	423.66
MOPSO	5374.306	7451.974	9	0.065	0.663	0.500	0.114	450.60
MOGWO	5472.983	7490.181	10	0.065	0.666	0.497	0.107	454.92
MOAHA	5157.460	6983.420	9	0.063	0.685	0.483	0.115	422.34

* A smaller MID (mean ideal distance) value reflects a closer proximity of the solution to the ideal point, ** A larger DM (diversity metric) value indicates better solution for diversity.

From the comparison results, it is obvious that the MOAHA algorithm outperforms the others in several aspects. A smaller MID value reflects a closer proximity of the Pareto front to the ideal point, thereby indicating better convergence performance of the proposed improved optimization algorithm. DM indicates the diversity of the solution, and higher values of DM are better, as they signify greater solution diversity. It can be observed that MOAHA achieves the lowest MID value and the highest DM value. Consequently, this study selects MOAHA as the candidate algorithm for further improvement and enhancement in the following research stages. However, when used alone, MOAHA may suffer from an inability to automatically select the best solution. These limitations can lead to subjective and time-consuming final solution selection from the Pareto set, resulting in sub-optimal planning decisions and ultimately reducing the cost-effectiveness and operational reliability of the microgrid in real-world applications. Hence, it is necessary to improve the MOAHA to achieve better performance.

4.3. Fuzzy Decision-Making

To support solution selection, this study integrates FDM with MOAHA. FDM does not objectively determine the universally best solution, instead, it evaluates and ranks the Pareto solutions based on predefined membership functions and preference weights. Therefore, the solution with the highest total membership value is regarded as the preferred configuration under the specified decision preference. In FDM, each objective is modeled using a linear membership function [16]. For an objective to be minimized, the membership function is expressed as follows:

$$\mu_r^i = \begin{cases} 1, & F_r^i \le F_{\min}^i \\ \frac{F_{\max}^i - F_r^i}{F_{\max}^i - F_{\min}^i}, & F_{\min}^i \le F_r^i \le F_{\max}^i \\ 0, & F_r^i \ge F_{\max}^i \end{cases} \tag{26}$$

where $F^i_{\min}$ and $F^i_{\max}$ are the minimum and maximum of the F_i objective function range, F^i_r and μ^i_r indicates the value of the ith objective function for the rth Pareto solution and the corresponding membership value, which reflects the quality of the ith objective in the rth Pareto solution. To calculate the total membership function for the rth Pareto solution, the corresponding individual membership functions are expressed as follows:

$$\mu_r = \frac{\sum_{i=1}^{m} \omega_i \mu_r^i}{\sum_{i=1}^{m} \omega_i} \tag{27}$$

where ω_i denotes the weighting factor associated with the *ith* objective function, determined based on specific requirements, and m refers to the number of objective functions. After calculating the total membership value for each Pareto solution, the solution with the highest total membership value is selected as the preferred solution under the specified preference weights.

5. Modes of Operation in Rule-Based Energy Management Strategy

A well-designed energy management strategy (EMS) is essential for the operation of hybrid renewable microgrid. This study proposed a rule-based EMS to program the components of microgrid system. This strategy follows the principles including (1) the electricity generated from renewable energy is first used to meet the load demand. If the renewable generation exceeds the load demand, the surplus will be stored in the battery energy storage system; (2) if the battery is fully charged, the additional surplus will be exported to the utility grid; (3) when renewable energy generation cannot meet the load demand, the battery is discharged to supply the demand shortfall; (4) if both renewable generation and battery cannot satisfy the load demand, electricity is imported from the utility grid to compensate for the shortfall. Table 2 presents the seven modes of operation for energy management considered in this study. These modes are designed based on practical power supply–demand relationships and predefined decision rules, aiming to ensure reliable load satisfaction, efficient utilization of renewable resources, and secure battery operation under different conditions.

Table 2. Summary of the seven modes of operation for energy management.

Mode No.	If Statement (Condition)	Then Statement (Action)
1	$P_{PV_out} + P_{WT_out} \geq P_{load}$, $SoC < SoC_{\max}$, without additional electricity.	$P_{PV_out} + P_{WT_out} \rightarrow P_{load} + P^{ch}_{BESS}$
2	$P_{PV_out} + P_{WT_out} \geq P_{load}$, $SoC < SoC_{\max}$, with additional electricity.	$P_{PV_out} + P_{WT_out} \rightarrow P_{load} + P^{ch}_{BESS} + P_{Grid_sell}$
3	$P_{PV_out} + P_{WT_out} \geq P_{load}$ and $SoC = SoC_{\max}$	$P_{PV_out} + P_{WT_out} \rightarrow P_{load} + P_{Grid_sell}$
4	$P_{PV_out} + P_{WT_out} < P_{load}$ and $SoC > SoC_{\text{healthy}}$	$P_{PV_out} + P_{WT_out} + P^{dis}_{BESS} \rightarrow P_{load}$
5	$P_{PV_out} + P_{WT_out} + P_{BESS} < P_{load}$ and $SoC > SoC_{\text{healthy}}$, during peak demand	$P_{PV_out} + P_{WT_out} + P^{dis}_{BESS} + P_{Grid_pur} \rightarrow P_{load}$
6	$P_{PV_out} + P_{WT_out} < P_{load}$ and $SoC \leq SoC_{\min}$	$P_{PV_out} + P_{WT_out} + P_{Grid_pur} \rightarrow P_{load} + P^{ch}_{BESS}$
7	$P_{PV_out} + P_{WT_out} < P_{load}$, grid outage, and $0 < SoC < SoC_{\max}$	$P_{PV_out} + P_{WT_out} + P^{dis}_{BESS} \rightarrow P_{load}$ until $SoC = 0$

6. Proposed Digital Twin Architecture for Microgrid

Digital twin technology has been successfully applied in sectors such as aerospace, industry, and transportation, where it supports operational monitoring, performance improvement, cost reduction, and enhanced safety and reliability. These applications demonstrate their potential for improving system digitalization and intelligence.

In the field of hybrid renewable energy microgrid planning, most existing sizing optimization studies mainly focus on obtaining static optimal configurations. Limited attention has been paid to how the optimized configuration can be dynamically mapped, monitored, and validated under different operating conditions. Therefore, the application of digital twin technology to the dynamic validation of static microgrid sizing results is still at an early stage.

To bridge this gap, this study proposed a digital twin architecture for hybrid renewable energy microgrids, as illustrated in Figure 3 [17,18]. The proposed architecture maps the optimized configuration into a dynamic virtual environment, enabling state and operational visualization, and validation of the planning result.

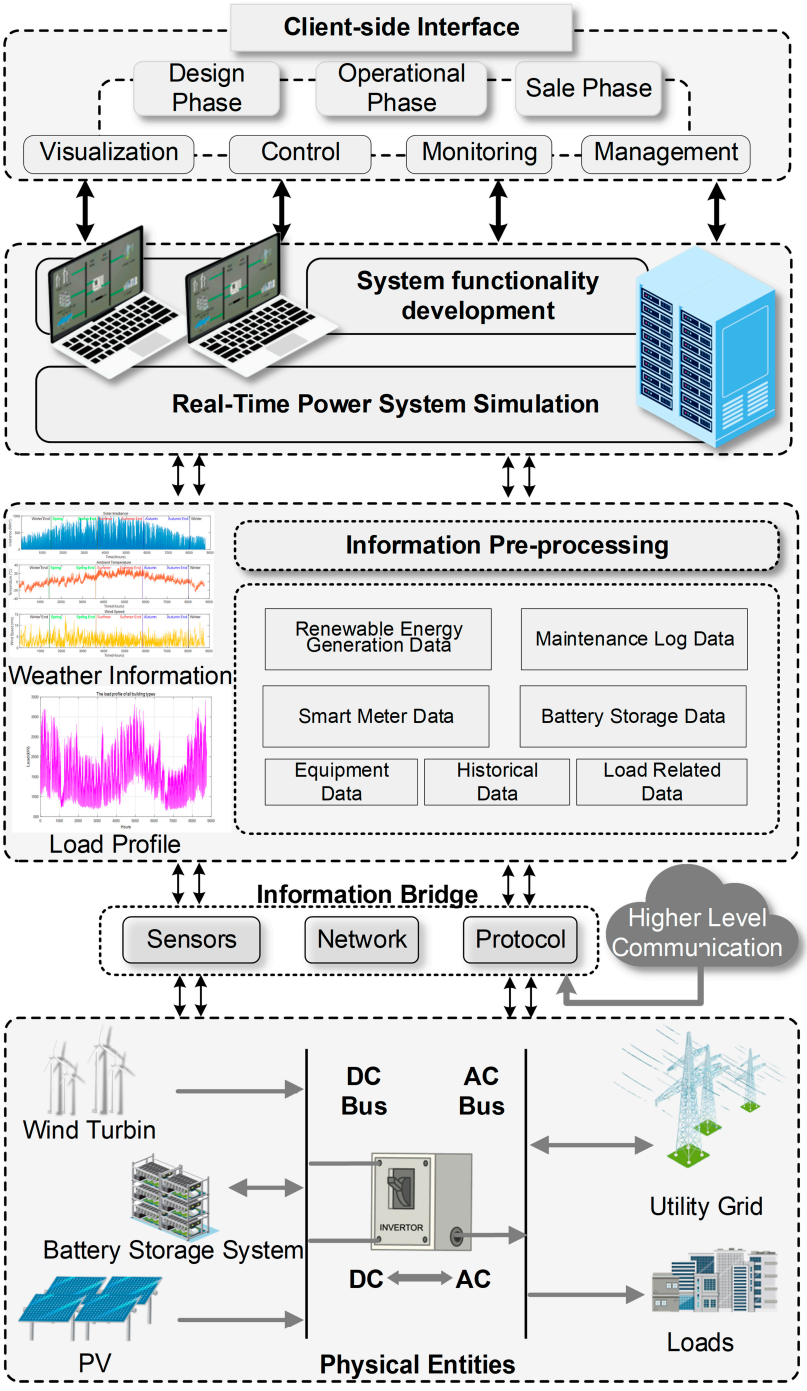


Figure 3. Proposed digital twin architecture for hybrid renewable energy microgrid.

The digital twin system usually contains three components: physical space (physical entities and connectivity), virtual space (virtual entities and services), and information processing (data). The physical space includes both the physical components and interconnections. In a hybrid renewable energy microgrid digital twin system, the component layer primarily consists of PV, WT, BESS, the utility grid, and inverters. These physical devices together form the foundation of the microgrid's energy supply and regulation system. The communication layer serves as a critical bridge in the framework. It connects the component layer to the information layer, ensuring seamless data exchange both among physical devices and between the physical space and the data layer. It facilitates this exchange through standardized protocols and middleware, thereby ensuring interoperability and real-time responsiveness. The information layer corresponds to the data of the digital twin. In the context of a hybrid renewable microgrid digital twin, this includes load demand, renewable energy generation data, and weather data. The core role of this layer is to collect, store, manage, and pre-process original data to support decision-making and optimization of the microgrid system. The virtual space of the digital twin includes virtual entities and services. The function layer in the digital twin system enables capabilities such as real-time simulation and display. These functions rely on both historical and real-time data from the information layer, and the results of analysis are passed upward to the business layer. Based on the analytical outputs, the business layer includes the planning, operational management, and market participation of the digital twin within the hybrid renewable energy microgrid. Its primary objective is to enhance the economic efficiency and sustainability of the microgrid system, while offering intelligent decision support for operators, users, and policymakers.

7. Location of the Case Study and Input Parameters

Urumqi, located in northwest inland China, has abundant solar radiation and good wind solar resource potential. Nevertheless, its energy structure is still dominated by fossil fuels, and the utilization of renewable energy remains relatively limited. Therefore, Urumqi provides a representative case for studying low-carbon energy planning for industrial users in resource rich but fossil fuel-dependent regions. To evaluate the performance of the proposed combined optimization strategy, this study implemented it to a hybrid renewable energy microgrid of an industrial park in Urumqi. The hourly meteorological data, including solar irradiation, ambient temperature, and wind speed, were collected from 1 January to 31 December 2023 in Urumqi, as illustrated in Figure 4. The annual load demand of an industrial park in Urumqi is provided in Figure 5. Table 3 refers to the technical and economic parameters of the microgrid components. During optimization process, the population size was 50, and the iteration number was 100.

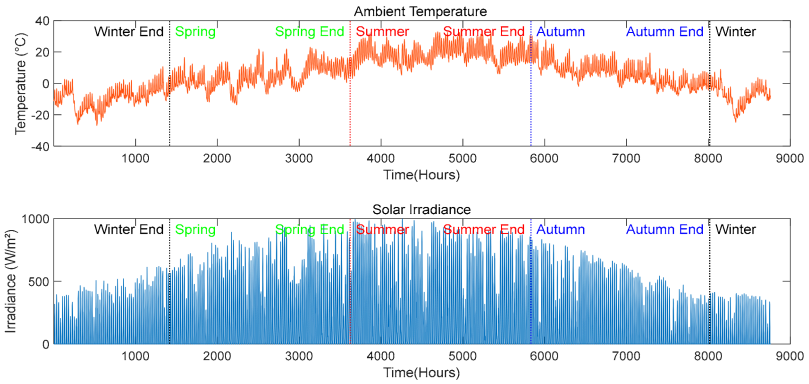


Figure 4. *Cont.*

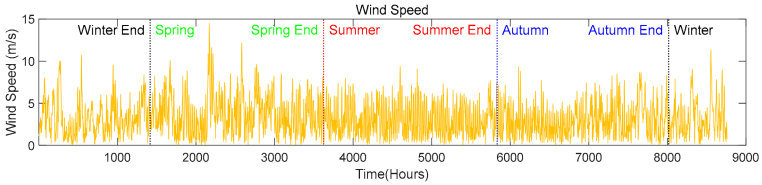


Figure 4. Annual time-series profiles of temperature, solar irradiance, and wind speed in Urumqi [19].

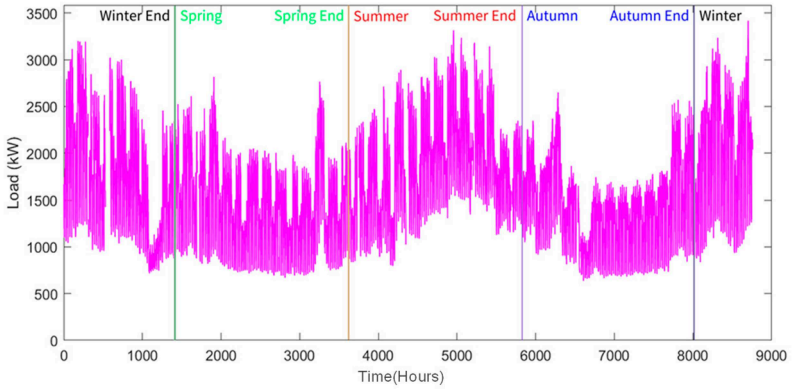


Figure 5. The annual load profile of an industrial park in Urumqi [20].

Table 3. Technical and economic parameters of the hybrid renewable microgrid components.

Components	Parameters		Value	Unit
PV Unit (LONGi Hi-MOX7) [21]	Regulator cost		1000	$
	Rated power		645	W
	Price		540	$/kW
	Regulator efficiency		98.8	%
	Life-time		25	year
Wind Turbine (GE 1.5 s) [22]	Price		1300	$/kW
	Rated power		600	kW
	Rated speed		11.5	m/s
	Cut-in speed		3.5	m/s
	Cut-out speed		25	m/s
	Efficiency		92	%
	Regulator cost		1200	$
	Life-time		25	year
Battery Storage System [23,24]	Rated power		40	kW
	Initial cost		108	$/kWh
	Battery efficiency		85	%
	Replacement cost		108	$/kWh
	Life-time		12	year
Utility Grid [25]	Import price (purchase)	8:00–11:00, 19:00–24:00	0.082	$/kWh
		0:00–4:00, 11:00–13:00, 17:00–19:00	0.062	$/kWh
		4:00–8:00, 13:00–17:00	0.045	$/kWh
	Export price (sell)	00:00–24:00	0.035	$/kWh
Inverter [23,26]	Initial cost		1500	$
	Efficiency		92	%
	Life-time		24	year
Economic Parameters [23]	O&M + running cost		5	%
	Real interest		13	%
	Discount rate		5	%
	Project life-time		24	year

8. Results and Discussion

8.1. Optimization Results

Since the sizing problem is formulated as a multi-objective optimization problem, the obtained Pareto front contains multiple non-dominated solutions with different trade-offs between COE and REF, as shown in Figure 6. To further support decision-making, representative Pareto solutions are evaluated and ranked using FDM, as shown in Figure 7. According to the FDM ranking under the specified preference weights, the first-ranked solution is selected as the preferred configuration. The selected configuration consists of 5357.450 kW PV, 7441.467 kWh BESS, and 10 wind turbines, achieving a COE of 0.065 $/kWh and an REF of 0.675. The annual power generated from PV and WT is illustrated in Figure 8 and Figure 9, respectively, and the monthly renewable generation comparison is presented in Figure 10.

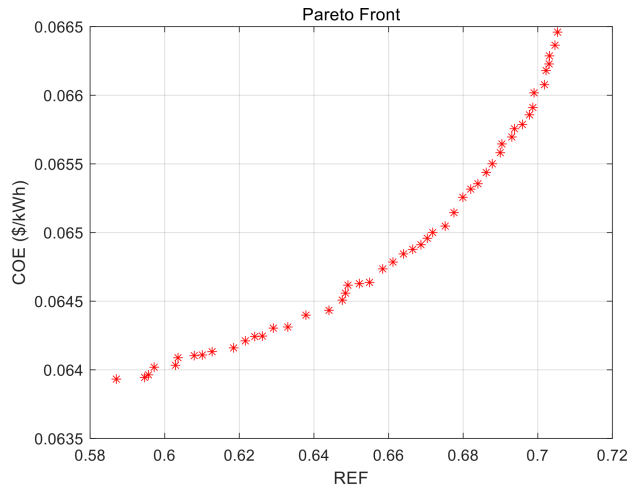


Figure 6. The optimal Pareto front generated by MOAHA, red asterisks represent non-dominated candidate solutions on the Pareto front.

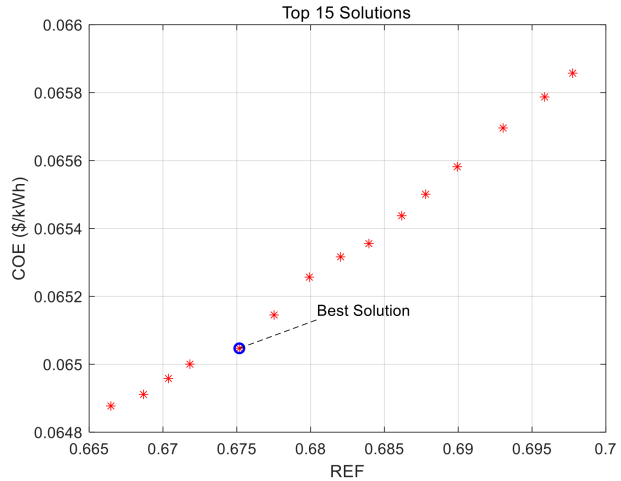


Figure 7. FDM ranking results of 15 representative Pareto solutions, red asterisks represent non-dominated candidate solutions on the Pareto front.

Figure 11a shows the annual power generation from PV, WT, and a battery system, along with the load demand of the system. Figure 11b presents a zoomed-in view of one typical week from Figure 11a, showing the hourly operation details. It can be seen that the RB-EMS effectively manages the operation of the proposed microgrid. It responds to changes in renewable generation and load demand, ensuring balanced energy supply and stable system operation.

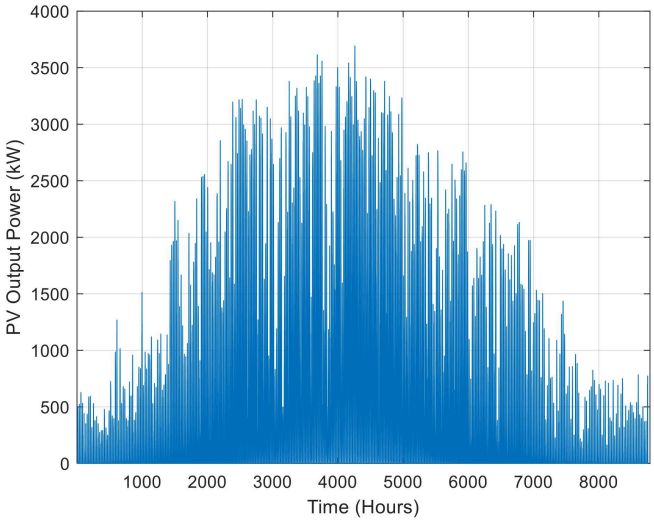


Figure 8. Generated output power from PV on the DC side for Urumqi for one year.

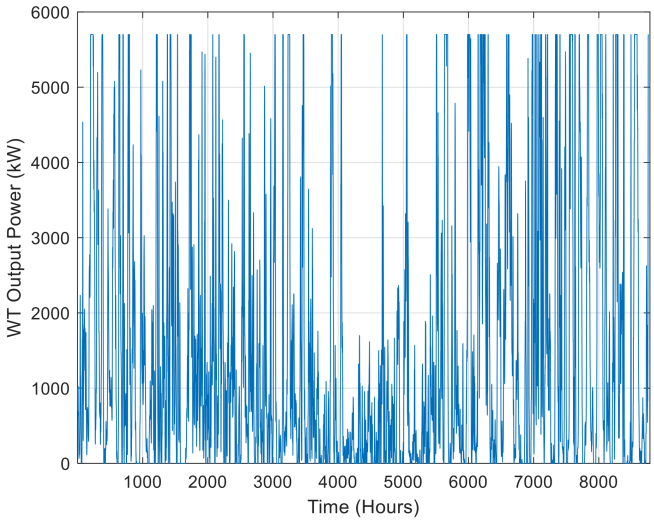


Figure 9. Generated output power from WT for Urumqi for one year.

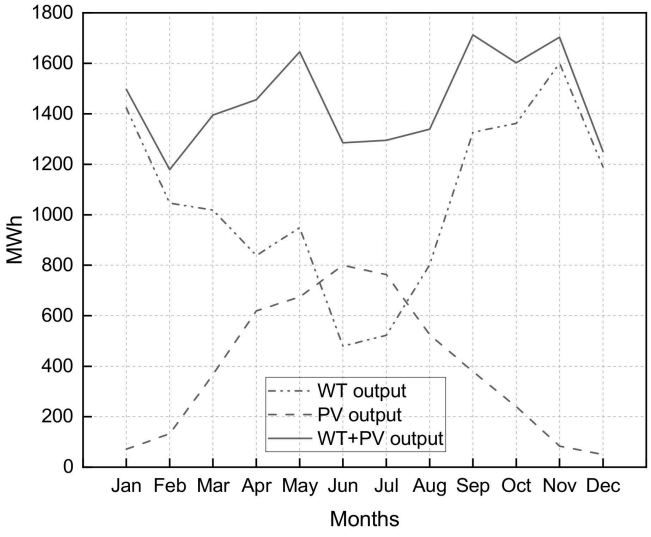


Figure 10. Monthly output power from renewable energy sources.

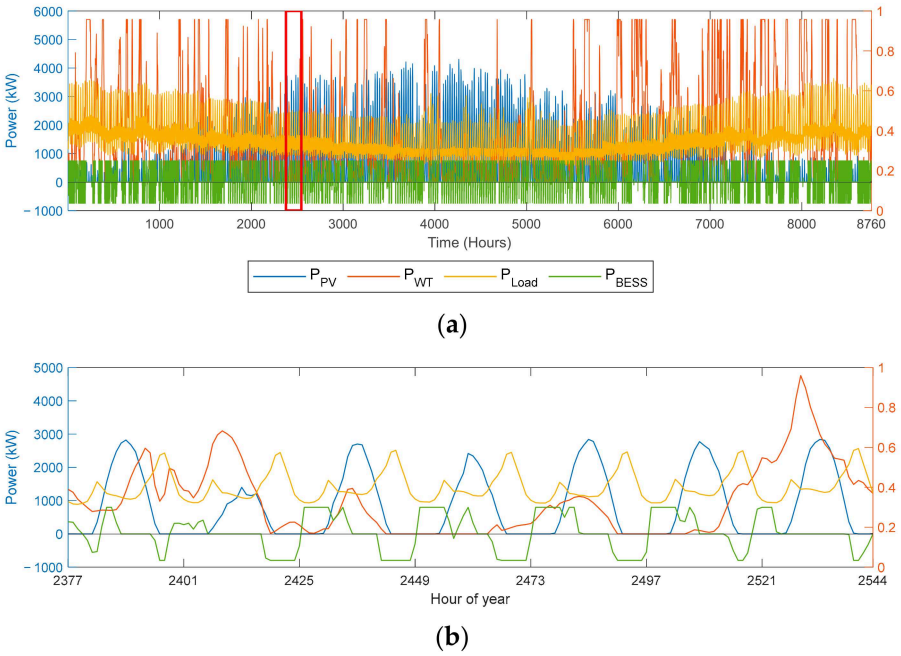


Figure 11. Electricity generated (**a**) annually charge/discharge, and load for one year; (**b**) zoomed-in view of the dotted frame in (**a**).

Figure 12a shows the battery SOC variation over the 8760 h of the year 2023. Figure 12b illustrates the battery SOC variations over 1 week in different seasons. By comparing the fluctuation range and frequency of the SOC curves, it is possible to assess the seasonal difference in battery utilization. In spring, the SOC fluctuates frequently and reaches both the minimum and maximum limits, indicating that the battery is actively involved in both charging and discharging. This leads to a high utilization rate. In summer, the SOC remains high and often reaches the maximum limit, meaning that the battery stays fully charged for long periods due to high solar radiation. As a result, the battery is less utilized. In autumn, moderate SOC variation is observed, suggesting a balanced use of the battery. In winter, the SOC frequently drops near the minimum level, indicating that the battery is often discharged to meet the demand. The utilization is high but mostly due to discharging.

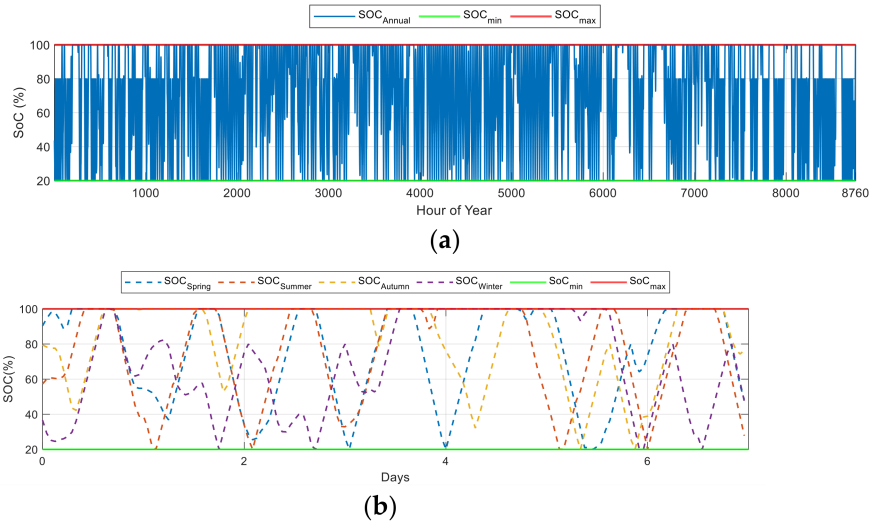


Figure 12. The state of charge of the battery (**a**) annually and (**b**) weekly for four seasons.

In short, battery utilization is highest in winter and spring, moderate in autumn, and lowest in summer. These seasonal differences reflect the variability of renewable energy generation and load demand and demonstrate the effectiveness of the proposed RB-EMS strategy under different seasonal conditions.

To verify the superiority and robustness of the proposed optimization strategy, a comparative analysis was conducted using three representative multi-objective optimization algorithms, namely the non-dominated sorting genetic algorithm II (NSGA-II), multi-objective particle swarm optimization (MOPSO), and multi-objective grey wolf optimizer (MOGWO). To reduce the influence of stochastic variations, each algorithm was independently executed 20 times under the same parameter settings. For each run, the fuzzy decision-making method was used to select the final compromise solution from the obtained Pareto front. The mean and standard deviation of PV capacity, BESS capacity, WT number, COE, REF, MID, DM, and computational time are reported in Table 4.

Table 4. Performance comparison of the proposed optimization strategy and benchmark algorithms over 20 independent runs.

Algorithm	PV (kW)	BESS (kWh)	WT (Unit)	COE ($/kWh)
NSGA-II	5534.46 ± 295.76	7456.88 ± 12.74	10 ± 0.49	0.0653 ± 0.0004
MOPSO	5309.70 ± 225.29	7447.88 ± 13.10	10 ± 0.22	0.0651 ± 0.0001
MOGWO	5548.40 ± 282.29	7467.46 ± 32.5	10 ± 0.41	0.0652 ± 0.0001
Proposed Optimization Strategy	5375.74 ± 244.90	7461.15 ± 19.47	10 ± 0.41	0.0651 ± 0.0001
Algorithm	REF	MID *	DM **	Run time (s)
NSGA-II	0.6837 ± 0.0098	0.6414 ± 0.0866	0.0855 ± 0.0202	423.28 ± 22.57
MOPSO	0.6785 ± 0.0033	0.5376 ± 0.0263	0.1172 ± 0.0038	450.69 ± 27.98
MOGWO	0.6803 ± 0.0030	0.5605 ± 0.0294	0.1151 ± 0.0072	454.71 ± 23.26
Proposed Optimization Strategy	0.6782 ± 0.0040	0.5324 ± 0.0345	0.1215 ± 0.0074	418.04 ± 26.64

* A smaller MID (mean ideal distance) value reflects a closer proximity of the solution to the ideal point, ** A larger DM (diversity metric) value indicates better solution for diversity.

The comparative results in Table 4 demonstrate the statistical robustness and practical advantage of the proposed optimization framework. The proposed strategy achieves the lowest MID value of 0.5324 ± 0.0345, indicating better convergence toward the ideal point than NSGA-II, MOPSO, and MOGWO. It also obtains the highest DM value of 0.1215 ± 0.0074, suggesting better solution diversity. Although the COE and REF values of the four algorithms are relatively close, the proposed strategy maintains a low COE of 0.0651 ± 0.0001 $/kWh with stable performance across repeated runs. In addition, it requires the shortest average runtime of 418.04 ± 26.64 s. These results indicate that the proposed MOAHA-FDM framework provides a better overall balance among convergence, diversity, economic performance, and computational efficiency.

To further examine whether the performance differences among the algorithms were statistically significant, the Kruskal–Wallis test was conducted based on the results of 20 independent runs [27]. A significance level of 0.05 was used. The results are presented in Table 5.

Table 5. Kruskal–Wallis test results for performance differences among different optimization algorithms.

Indicator	Chi-Square	df	*p*-Value	Significant at $p < 0.05$
COE ($/kWh)	8.6794	3	0.0339	Yes
REF	7.5333	3	0.0567	No
MID *	31.2967	3	7.3616	Yes
DM **	41.5326	3	5.0414	Yes
Run time (s)	55.4783	3	5.4283	Yes

* A smaller MID (mean ideal distance) value reflects a closer proximity of the solution to the ideal point, ** A larger DM (diversity metric) value indicates better solution for diversity.

The Kruskal–Wallis test results in Table 5 indicate that significant differences exist among the four algorithms for COE, MID, DM, and computational time, with *p*-values lower than 0.05. However, no statistically significant difference is observed for REF, suggesting that the renewable energy fraction obtained by the four algorithms is relatively comparable. These results further confirm that the proposed MOAHA-FDM framework shows statistically distinguishable performance in terms of convergence, diversity, and computational efficiency. Combined with the mean and standard deviation results in Table 4, the proposed strategy provides a stable and competitive optimization performance for microgrid planning.

8.2. Seasonal Operating Scenario Analysis

To further discuss the applicability of the proposed framework, a seasonal operating scenario analysis was conducted. Four representative 48 h periods were selected from winter, spring, summer, and autumn to reflect different combinations of renewable generation and load conditions.

The selected seasonal scenarios represent different operating challenges for the microgrid. Winter is characterized by low solar irradiance and relatively high wind speed, where wind generation and grid support play a more important role. Spring generally has both higher solar irradiance and wind speed, leading to frequent renewable surplus and battery charging or grid selling. Summer is dominated by PV generation because of strong solar irradiance and relatively low wind speed, while autumn shows weaker renewable generation and, therefore, requires more coordination among renewable sources, BESS, and the utility grid. By comparing the operating modes, battery charge/discharge behavior, grid purchase/selling power, and load-following performance across these four seasonal scenarios, the applicability of the optimized configuration and the proposed RB-EMS under diverse operating conditions can be further examined.

8.2.1. Winter Operating Scenario Analysis

Winter occurs at the beginning and end of the year, corresponding to hours 1–1416 and 8040–8760. The first two days of the year were selected as a representative winter operating scenario, as shown in Figure 13.

During this period, PV generation remains very limited, especially during the early morning hours, while WT output contributes a major share of renewable generation. When WT generation and battery discharge are sufficient, the load demand can be supplied by renewable energy and the BESS. When the combined renewable generation and battery discharge are insufficient, the system switches to grid-supported operation. In some hours, the battery reaches its minimum SOC and cannot continue discharging; therefore, the utility grid is used not only to supply the load but also to charge the battery until the healthy SOC level is restored. These results indicate that the proposed RB-EMS can maintain feasible

operation in winter by coordinating WT generation, BESS operation, and grid purchase under low PV conditions.

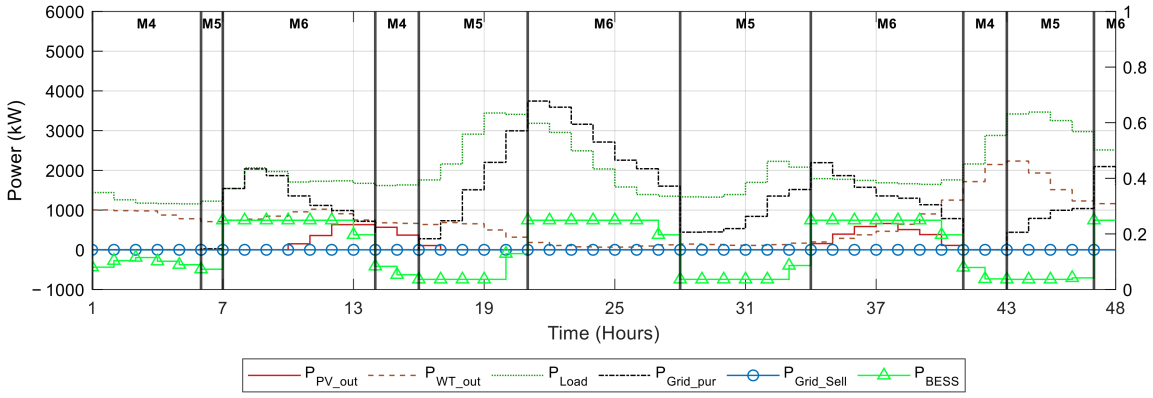


Figure 13. Daily output electricity generation in winter.

8.2.2. Spring Operating Scenario Analysis

Spring covers March to May, corresponding to hours 1417–3647. The period from 1969 to 2016 was selected as a representative spring operating scenario, as shown in Figure 14. In this period, the system first operates in grid-supported mode when the combined renewable generation and battery discharge are insufficient to meet the load demand. When the battery reaches its minimum SOC, the utility grid supplies the load and charges the battery until the healthy SOC level is restored. As PV and WT output increase, renewable generation exceeds the load demand, and the surplus electricity is first used to charge the battery. When the battery charging limit or maximum SOC is reached, the remaining surplus energy is exported to the utility grid. When renewable generation decreases again, the battery discharges to support the load, and the system switches back to grid-supported operation when necessary. These results indicate that, under spring conditions with relatively abundant renewable resources, the proposed RB-EMS can effectively coordinate PV, WT, BESS, and the utility grid to improve renewable energy utilization while maintaining reliable load supply and safe battery operation.

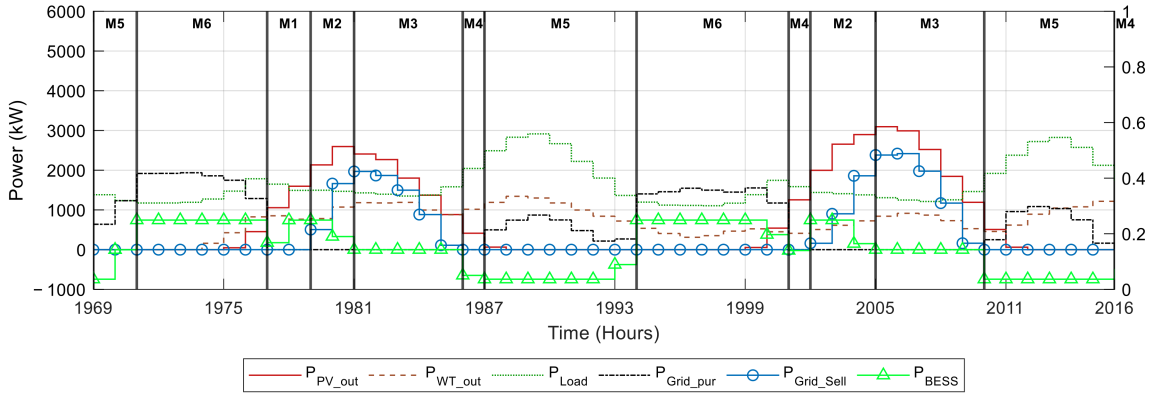


Figure 14. Daily output electricity generation in spring.

8.2.3. Summer Operating Scenario Analysis

Summer covers June to August, corresponding to hours 3648–5855. The period from hour 4537 to hour 4584 was selected as a representative summer operating scenario, as shown in Figure 15. During this period, the system first operates in grid-supported mode when renewable generation and battery discharge are insufficient to meet the load demand. As PV output increases rapidly, renewable generation exceeds the load demand, and the

surplus electricity is used to charge the battery. When the battery charging power limit or maximum SOC is reached, the remaining surplus electricity is exported to the utility grid. After PV generation decreases, the battery discharges to support the load, and the system switches back to grid-supported operation when necessary. These results show that, under PV-dominated summer conditions, the proposed RB-EMS can flexibly coordinate PV generation, BESS operation, and grid interaction to absorb surplus renewable energy and maintain reliable load supply.

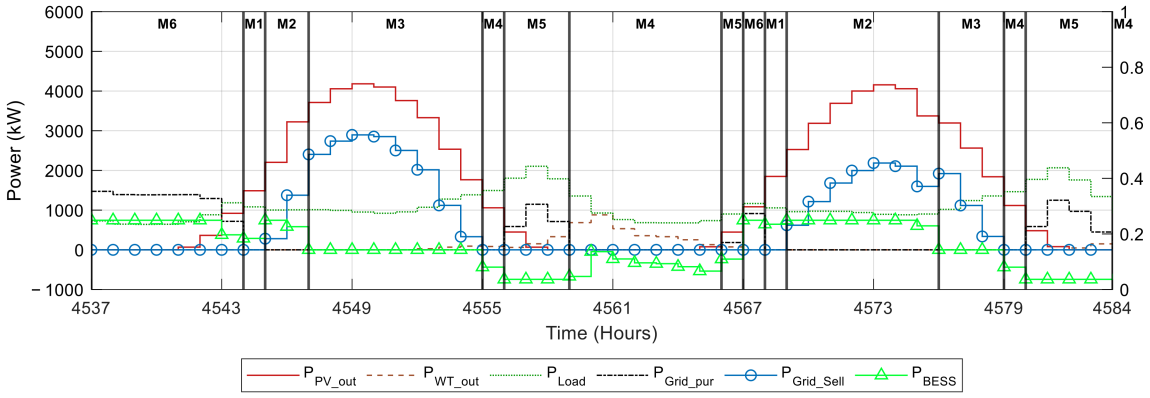


Figure 15. Daily output electricity generation in summer.

8.2.4. Autumn Operating Scenario Analysis

Autumn (the mild season) is the fourth season of the year. The simulation focuses on hours 6697 to 6744, and further analysis is presented in Figure 16. During this period, renewable generation fluctuates considerably, leading to frequent switching among different operating modes. When the combined PV, WT, and BESS output is insufficient to meet the load demand, the system operates in grid-supported mode. When the battery reaches its lower SOC threshold, the utility grid supplies the load and charges the battery to restore a healthy SOC level. As PV and WT output increase, surplus renewable energy is first used to charge the BESS, and the remaining surplus is exported to the grid when charging constraints are reached. When renewable generation decreases again, the BESS discharges to support the load, while grid power is purchased when necessary. These results indicate that the proposed RB-EMS can effectively coordinate PV, WT, BESS, and the utility grid under autumn conditions with variable renewable generation, thereby maintaining reliable load supply and safe battery operation.

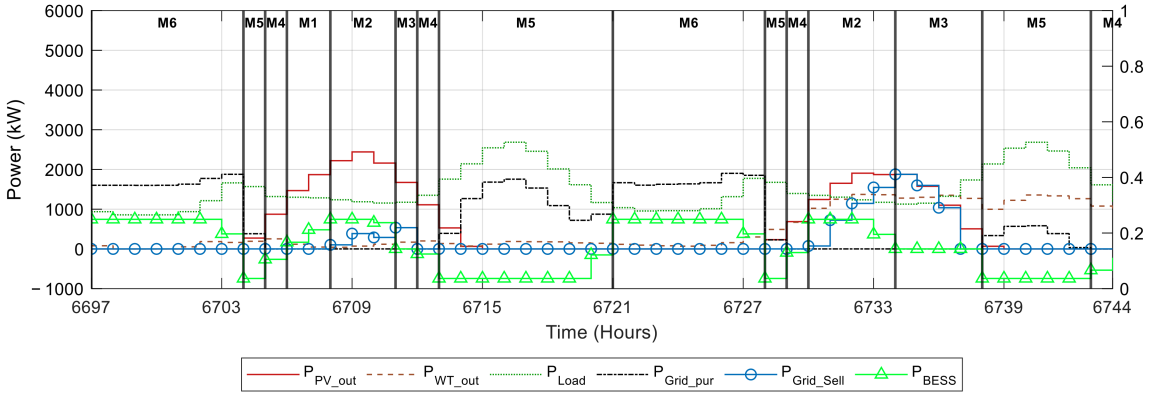


Figure 16. Daily output electricity generation in autumn.

These results indicate that the selected configuration is not only feasible under a single operating condition but can also adapt to different seasonal renewable generation patterns through coordinated operation of PV, WT, BESS, and the utility grid.

8.3. Sensitivity Analysis

To evaluate the influence of renewable generation and load uncertainties on the selected configuration, a sensitivity analysis was conducted. The optimized configuration obtained from the proposed MOAHA-FDM framework was kept unchanged, and the annual solar irradiance, wind speed, and load demand profiles were adjusted under different uncertainty scenarios. The base case represents the original deterministic profiles used in the optimization process. In S1, solar irradiance and wind speed were reduced by 10%, while the load demand was increased by 10%, representing a moderate adverse condition. In S2, solar irradiance and wind speed were reduced by 20%, while the load demand was increased by 15%, representing a more severe adverse condition. In S3, solar irradiance and wind speed were increased by 10%, while the load demand was reduced by 10%, representing a renewable surplus condition. The changes in COE, REF, grid import energy, and grid export energy relative to the base case are shown in Figure 17.

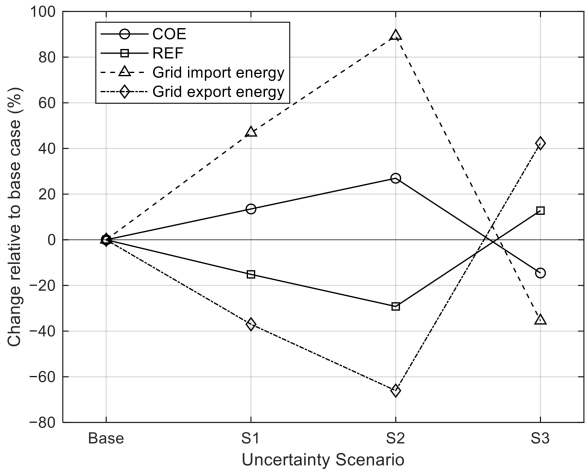


Figure 17. Uncertainty analysis of the selected configuration under renewable generation and load variations.

As shown in Figure 17, renewable generation and load uncertainties have a clear influence on the economic and operational performance of the selected microgrid configuration. Under the scenarios S1 and S2, the reduction in renewable generation and the increase in load demand led to higher COE and greater dependence on grid import energy. In S1, COE increases by approximately 13%, while grid import energy increases by about 45%. Meanwhile, REF decreases by around 15%, and grid export energy decreases by about 37%. These results indicate that even moderate renewable load uncertainty can reduce renewable energy utilization and increase the need for electricity purchased from the utility grid.

The impact becomes more significant under the scenario S2. Compared with the base case, COE increases by approximately 26%, and grid import energy increases by around 85%. At the same time, REF decreases by nearly 29%, and grid export energy decreases by approximately 65%. This indicates that when renewable generation is substantially lower and load demand is higher, the microgrid relies more heavily on the utility grid to maintain the power balance. Therefore, renewable generation and load uncertainties may significantly affect the economic performance and renewable energy utilization of the optimized configuration.

In contrast, S3 shows the opposite trend. When renewable generation increases and load demand decreases, COE is reduced by approximately 14%, while REF increases by around 13%. Grid import energy decreases by about 34%, whereas grid export energy increases by more than 40%. This demonstrates that renewable surplus conditions can improve the economic and environmental performance of the system by reducing grid dependence and increasing the amount of energy exported to the utility grid.

Overall, the sensitivity analysis confirms that renewable generation and load uncertainties can considerably affect COE, REF, and grid interaction behavior. Although the proposed optimization model is based on deterministic weather and load profiles, the scenario analysis provides additional insight into the operational robustness of the selected configuration under different uncertainty conditions. The results also suggest that future research should further incorporate stochastic or robust optimization methods to explicitly consider renewable generation and load uncertainties during the planning stage.

8.4. Digital Twin System

Based on the proposed digital twin architecture, a digital twin system was developed for an industrial park microgrid in Urumqi, as shown in Figure 18. The digital twin system provides several practical insights for microgrid operation and management. The left panel presents the key performance indicators of the optimized configuration, such as COE, REF, annual energy purchase, annual energy selling, and curtailment. The lower-left panel shows the battery energy, SOC, and current operating mode, which helps evaluate whether the BESS operates within a safe and reasonable range. The upper panel displays the current simulation time and operating variables, including PV output, WT output, load demand, grid purchase, grid selling, and simulation step. The right panel presents the last-48 h trends of PV/WT/load, SOC, and grid buy/sell power, which allows users to observe the dynamic response of the microgrid to renewable energy fluctuations and load variations. Therefore, Figure 13 demonstrates how the digital twin system transforms static optimization results into observable operational states and provides a practical basis for checking power balance, SOC constraints, grid interaction behavior, and the feasibility of the selected configuration.

More importantly, this system is not only a visualization interface, but also an important link between the optimization results and the operational validation process. In the proposed framework, the MOAHA-FDM optimization stage first determines the static sizing configuration, including the PV capacity, BESS capacity, and the number of WTs. These optimized sizing results are then imported into the rule-based energy management strategy and the digital twin platform. The scheduling model calculates the hourly operating states of the microgrid, including renewable generation, load demand, battery charging and discharging, SOC variation, grid power purchase, grid power selling, and operation mode. The digital twin system maps these scheduling outputs into a virtual environment, allowing the optimized configuration to be dynamically observed and validated under time-varying operating conditions.

Therefore, the optimized static configuration is not directly regarded as the final practical solution. Instead, it is further mapped into a time-series operating environment through the rule-based EMS and the digital twin system. This process enables the dynamic feasibility of the optimized configuration to be verified under hourly variations in renewable generation and load demand.

From the perspective of system development, the proposed digital twin system provides a virtual testbed for transforming optimization results into observable and executable operating processes. In the design stage, the system allows developers to examine whether the selected PV capacity, WT number, and BESS capacity can satisfy load demand while

maintaining SOC constraints and reasonable grid interaction behavior. Compared with directly testing different configurations in a physical microgrid, this virtual validation process can reduce repeated trial-and-error, shorten the design iteration cycle, and lower the potential cost and risk of system deployment. In addition, the modular structure of the digital twin system makes it convenient to update component parameters, import new scheduling results, or modify the EMS logic. Existing optimization and scheduling programs developed in MATLAB can also be migrated or connected to the digital twin platform through data interfaces, which improves code reusability and avoids rebuilding the entire simulation process from the beginning.



Figure 18. Digital twin system for the hybrid microgrid in the industrial park.

For operators and system managers, the developed system improves the interpretability and usability of the optimization results. Traditional optimization outputs are usually presented as numerical tables or static curves, which makes it difficult to understand how the microgrid actually operates over time. In contrast, the digital twin system converts these results into dynamic operating states and visual energy-flow information. Operators can directly observe whether renewable generation is sufficient, when the battery is charged or discharged, and when the microgrid needs to purchase electricity from or sell electricity to the utility grid. This helps identify potential problems such as excessive grid dependence, unreasonable battery operation, SOC boundary risks, or renewable energy surplus. Therefore, the system can support operation analysis, schedule checking, and energy management before practical implementation.

For end-users, the system reduces the technical barrier to understanding microgrid operation. Instead of relying only on mathematical models and optimization indicators, users can intuitively observe the relationship among renewable generation, load demand, battery SOC, and grid interaction. This improves the transparency of the planning results and helps users understand why a specific configuration or scheduling strategy is selected. In practical applications, such visualization can support communication among planners, op-

erators, and decision makers, especially when evaluating whether the proposed microgrid scheme is technically feasible, economically reasonable, and operationally reliable.

In this study, dynamic validation is mainly reflected in the time-series verification of power balance, SOC constraints, and grid interaction behavior. By observing the hourly PV output, WT output, load demand, battery SOC, and grid import/export power, the system verifies whether the optimized configuration can operate feasibly under variable renewable generation and load conditions. Therefore, the developed digital twin system not only makes the optimization results easier to understand, but also provides a practical tool for configuration validation, operation analysis, schedule verification, and energy management of industrial park microgrids.

Although the developed digital twin system can dynamically visualize the operating states of the optimized microgrid configuration and provide preliminary feasibility verification under time-series renewable generation and load conditions, it should be acknowledged that the current system is mainly designed as a digital twin visualization and verification platform rather than a fully closed-loop digital twin. Its primary functions are to map the optimized static configuration into a time-series virtual operating environment and to support virtual representation, data mapping, operational visualization, and pre-implementation feasibility checking. However, a comprehensive quantitative performance validation of the digital twin platform has not yet been fully conducted at this stage. Rigorous validation metrics, such as MAE, RMSE, NRMSE, R^2, power balance residual, SOC violation rate, communication latency, and physical to virtual synchronization accuracy, were not fully evaluated using measured operational data. In addition, full bidirectional synchronization between the physical microgrid and the virtual model, online model updating, predictive operation analysis, and closed-loop control have not yet been implemented in the current system. Therefore, future work will further improve the proposed digital twin framework by integrating real-time data acquisition, measured operational data, online parameter updating, quantitative validation metrics, predictive analysis, and closed-loop control strategies, so as to more rigorously assess the accuracy, robustness, synchronization performance, and real-time applicability of the digital twin system for intelligent microgrid management.

8.5. Implications of the Proposed Framework

From a management science perspective, the proposed MOAHA-FDM framework is not only an optimization tool, but also a decision-support method for practical microgrid planning and management. In industrial park energy systems, managers are often required to make investment and planning decisions under multiple conflicting objectives, such as reducing energy cost, increasing renewable energy utilization, maintaining power supply reliability, and controlling equipment investment. The proposed framework supports this process by converting the technical sizing problem into a structured multi-objective decision-making problem.

First, the framework supports decision-making by providing a set of Pareto-optimal configurations and further ranking them through FDM according to predefined preference weights. This allows decision-makers to explicitly express their preferences between economic cost and renewable energy utilization. Therefore, the final configuration is not selected only by subjective judgment, but through a transparent and repeatable decision-making process.

Furthermore, the framework supports resource allocation by determining the installed capacity of PV, the capacity of BESS, and the number of WTs. These decision variables directly correspond to investment allocation among different energy resources. By comparing different trade-off solutions, managers can understand how increasing or reducing

investment in renewable generation and storage affects the overall cost and renewable energy factor of the microgrid.

Additionally, the proposed framework supports operational management when combined with the rule-based EMS and digital twin system. The optimized configuration can be mapped into a time-series operating environment, where PV output, WT output, load demand, battery SOC, and grid import/export power can be observed dynamically. This helps operators identify potential management issues, such as excessive dependence on the utility grid, unreasonable battery charging or discharging behavior, SOC boundary risks, and renewable energy surplus.

Finally, the framework supports sustainable energy planning by linking economic performance with renewable energy utilization. The COE objective reflects the economic feasibility of the planning scheme, while the REF objective reflects the contribution of renewable energy to the energy supply. Therefore, the proposed methodology can help industrial park managers develop a more balanced and sustainable energy planning strategy that considers both cost-effectiveness and low-carbon energy transition.

9. Conclusions

This study proposed an integrated framework for the optimal planning and dynamic validation of a hybrid renewable energy microgrid. First, a combined optimization strategy integrating the multi-objective artificial hummingbird algorithm and fuzzy decision-making was developed to address the trade-off between economic cost and renewable energy utilization in microgrid planning. A multi-objective artificial hummingbird algorithm was employed to generate a well-distributed Pareto front, while Fuzzy decision-making was used to rank the candidate solutions and identify the preferred system configuration under the specified decision preference. In this way, both Pareto-front generation and final scheme selection were effectively addressed. Furthermore, to overcome the limitation that the selected planning scheme remains a static result, a digital twin architecture for the hybrid renewable energy microgrid was further proposed. Based on the optimized configuration, a corresponding digital twin system was developed to realize virtual representation, dynamic state mapping, operational visualization, and configuration validation under time-varying operating conditions. This extends the role of planning research from static optimal design to dynamic operational support and verification. Finally, a grid-connected industrial park microgrid in Urumqi was adopted as the case study. The preferred configuration consists of 5357.450 kW PV, 7441.467 kWh BESS, and 10 wind turbines, achieving a COE of 0.065 $/kWh and an REF of 0.675. Compared with NSGA-II, MOPSO, and MOGWO, the proposed strategy achieves the lowest MID, the highest DM, and the shortest average runtime over 20 independent runs, with statistically significant differences confirmed by the Kruskal–Wallis test. The results verified the effectiveness of the proposed optimization strategy in obtaining a balanced planning solution and demonstrated the capability of the developed digital twin system in reflecting and validating the dynamic operation of the optimized microgrid configuration. Therefore, the proposed framework not only improves the scientific ability and practicality of hybrid renewable energy microgrid planning, but also provides a feasible pathway for promoting digitalized, intelligent, and scalable energy system development from individual microgrid projects to broader industrial energy applications.

Author Contributions: Conceptualization, methodology, software, validation, writing—original draft preparation, S.L.; formal analysis, investigation, resources, data curation, funding acquisition, writing—review and editing, C.W.T.; visualization, supervision, project administration, N.T. All authors have read and agreed to the published version of the manuscript.

Funding: This research was funded by the Ministry of Higher Education under Fundamental Research Grant Scheme [FRGS/1/2023/TK08/UTM/02/43]. Also, co-funded by Istanbul Ticaret University.

Institutional Review Board Statement: Not applicable.

Informed Consent Statement: Not applicable.

Data Availability Statement: The data presented in this study are not publicly available due to institutional data management restrictions and confidentiality considerations. The data are available from the corresponding author upon reasonable request.

Conflicts of Interest: The authors declare no conflicts of interest.

References

1. Zidane, T.E.K.; Ab Muis, Z.; Ho, W.S.; Zahraoui, Y.; Aziz, A.S.; Su, C.-L.; Mekhilef, S.; Campana, P.E. Power systems and microgrids resilience enhancement strategies: A review. *Renew. Sustain. Energy Rev.* **2025**, *207*, 114953. [CrossRef]
2. Teimourzadeh, S.; Tor, O.B.; Cebeci, M.E.; Bara, A.; Oprea, S.V. A three-stage approach for resilience-constrained scheduling of networked microgrids. *J. Mod. Power Syst. Clean Energy* **2019**, *7*, 705–715. [CrossRef]
3. Jeyaraj, T.; Ponnusamy, A.; Selvaraj, D. Hybrid renewable energy systems stability analysis through future advancement technique: A review. *Appl. Energy* **2025**, *383*, 125355. [CrossRef]
4. Duan, F.; Eslami, M.; Khajehzadeh, M.; Basem, A.; Jasim, D.J.; Palani, S. Optimization of a photovoltaic/wind/battery energy-based microgrid in distribution network using machine learning and fuzzy multi-objective improved Kepler optimizer algorithms. *Sci. Rep.* **2024**, *14*, 13354. [CrossRef] [PubMed]
5. Samy, M.M.; Güven, A.F. Optimal dimensioning of grid-connected PV/wind hybrid renewable energy systems with battery and supercapacitor storage a statistical validation of meta-heuristic algorithm performance. *Sci. Rep.* **2025**, *15*, 45658. [CrossRef] [PubMed]
6. Ali, M.F.; Sheikh, M.R.I.; Akter, R.; Islam, K.N.; Ferdous, A.I. Grid-connected hybrid microgrids with PV/wind/battery: Sustainable energy solutions for rural education in Bangladesh. *Results Eng.* **2025**, *25*, 103774. [CrossRef]
7. Hossain, M.A.; Ahmed, A.; Tito, S.R.; Ahshan, R.; Sakib, T.H.; Nengroo, S.H. Multi-objective hybrid optimization for optimal sizing of a hybrid renewable power system for home applications. *Energies* **2022**, *16*, 96. [CrossRef]
8. Cheraghi, R.; Jahangir, M.H. Multi-objective optimization of a hybrid renewable energy system supplying a residential building using NSGA-II and MOPSO algorithms. *Energy Convers. Manag.* **2023**, *294*, 117515. [CrossRef]
9. Tezer, T. Multi-objective optimization of hybrid renewable energy systems with green hydrogen integration and hybrid storage strategies. *Int. J. Hydrogen Energy* **2025**, *142*, 1249–1271. [CrossRef]
10. Bernal-Agustín, J.L.; Dufo-López, R.; Rivas-Ascaso, D.M. Design of isolated hybrid systems minimizing costs and pollutant emissions. *Renew. Energy* **2006**, *31*, 2227–2244. [CrossRef]
11. Sheridan, L.M.; Phillips, C.; Orrell, A.C.; Berg, L.K.; Tinnesand, H.; Rai, R.K.; Zisman, S.; Duplyakin, D.; Flaherty, J.E. Validation of wind resource and energy production simulations for small wind turbines in the United States. *Wind Energy Sci.* **2022**, *7*, 659–676. [CrossRef]
12. Kaabeche, A.; Belhamel, M.; Ibtiouen, R. Sizing optimization of grid-independent hybrid photovoltaic/wind power generation system. *Energy* **2011**, *36*, 1214–1222. [CrossRef]
13. Ofak, Z.; Zupan, A.; Plavsic, T. Transmission Grid Connection of Energy Storage Facilities—Overview and Challenges. *Teh. Vjesn.—Tech. Gaz.* **2019**, *26*, 862–871.
14. Azaza, M.; Wallin, F. Multi objective particle swarm optimization of hybrid micro-grid system: A case study in Sweden. *Energy* **2017**, *123*, 108–118. [CrossRef]
15. Maghsoudlou, H.; Afshar-Nadjafi, B.; Niaki, S.T.A. A multi-objective invasive weeds optimization algorithm for solving multi-skill multi-mode resource constrained project scheduling problem. *Comput. Chem. Eng.* **2016**, *88*, 157–169. [CrossRef]
16. Norouzi, M.R.; Ahmadi, A.; Nezhad, A.E.; Ghaedi, A. Mixed integer programming of multi-objective security-constrained hydro/thermal unit commitment. *Renew. Sustain. Energy Rev.* **2014**, *29*, 911–923. [CrossRef]
17. Bazmohammadi, N.; Madary, A.; Vasquez, J.C.; Mohammadi, H.B.; Khan, B.; Wu, Y.; Guerrero, J.M. Microgrid Digital Twins: Concepts, Applications, and Future Trends. *IEEE Access* **2022**, *10*, 2284–2302. [CrossRef]
18. Kumari, N.; Sharma, A.; Tran, B.; Chilamkurti, N.; Alahakoon, D. A Comprehensive Review of Digital Twin Technology for Grid-Connected Microgrid Systems: State of the Art, Potential and Challenges Faced. *Energies* **2023**, *16*, 5525. [CrossRef]
19. National Aeronautics and Space Administration POWER Data Access Viewer. Available online: https://power.larc.nasa.gov/ (accessed on 3 January 2025).
20. Zhou, K. High resolution electric power load data of an industrial park with multiple types of buildings in China. *Sci. Data* **2023**, *10*, 870. [CrossRef] [PubMed]

21. LONGi Green Energy Technology Co., Ltd. Hi-MO X10 Photovoltaic Module Series. Available online: https://www.longi.com/en/products/modules-series/hi-mo-x10/ (accessed on 28 February 2025).
22. Xinjiang Goldwind Science & Technology Co., Ltd. Goldwind Wind Turbine Portfolio (Including GW155 Series). Available online: https://www.goldwind.com/cn/equipment/wind-turbine (accessed on 28 February 2025).
23. Heydari, A.; Nezhad, M.M.; Keynia, F.; Fekih, A.; Shahsavari-Pour, N.; Garcia, D.A.; Piras, G. A combined multi-objective intelligent optimization approach considering techno-economic and reliability factors for hybrid-renewable microgrid systems. *J. Clean. Prod.* **2023**, *383*, 135249. [CrossRef]
24. Bloomberg Lithium-Ion Battery Pack Prices Fall to $108 Per Kilowatt-Hour, Despite Rising Metal Prices: BloombergNEF. Available online: https://about.bnef.com/insights/clean-transport/lithium-ion-battery-pack-prices-fall-to-108-per-kilowatt-hour-despite-rising-metal-prices-bloombergnef/ (accessed on 22 February 2025).
25. Electricity Price List for Commercial and Industrial Users Purchased by State Grid Xinjiang Electric Power Co., Ltd. Available online: https://zhaopin.sgcc.com.cn/sgcchr/static/unitInfo.html?obj_id=10625124 (accessed on 11 March 2025).
26. Victron Energy. Inverter Smart. Available online: https://www.victronenergy.com/inverters/phoenix-inverter-smart#downloads-manuals (accessed on 16 February 2025).
27. Caban, J.; Nieoczym, A.; Krzywonos, L.; Drozd, K. Statistical analysis of vehicle repair costs in a transport company. *Transp. Res. Procedia* **2026**, *93*, 24–30. [CrossRef]

Disclaimer/Publisher's Note: The statements, opinions and data contained in all publications are solely those of the individual author(s) and contributor(s) and not of MDPI and/or the editor(s). MDPI and/or the editor(s) disclaim responsibility for any injury to people or property resulting from any ideas, methods, instructions or products referred to in the content.